Smart Structures and Systems, *Vol. 22, No. 2 (2018) 223-230*
DOI: https://doi.org/10.12989/sss.2018.22.2.223

High-speed angular-scan pulse-echo ultrasonic propagation imager for in situ non-destructive evaluation

Syed H. Abbas and Jung-Ryul Lee*

Department of Aerospace Engineering, Korean Advanced Institute for Science and Technology, 291 Daehak-ro, Yuseong-gu, Daejeon 305-701, Republic of Korea

(Received May 20, 2017, Revised November 18, 2017, Accepted November 28, 2017)

Abstract. This study examines a non-contact laser scanning-based ultrasound system, called an angular scan pulse-echo ultrasonic propagation imager (A-PE-UPI), that uses coincided laser beams for ultrasonic sensing and generation. A laser Doppler vibrometer is used for sensing, while a diode pumped solid state (DPSS) Q-switched laser is used for generation of thermoelastic waves. A high-speed raster scanning of up to 10-kHz is achieved using a galvano-motorized mirror scanner that allows for coincided sensing and for the generation beam to perform two-dimensional scanning without causing any harm to the surface under inspection. This process allows for the visualization of longitudinal wave propagation through-the-thickness. A pulse-echo ultrasonic wave propagation imaging algorithm (PE-UWPI) is used for on-the-fly damage visualization of the structure. The presented system is very effective for high-speed, localized, non-contact, and non-destructive inspection of aerospace structures. The system is tested on an aluminum honeycomb sandwich with disbonds and a carbon fiber-reinforced plastic (CFRP) honeycomb sandwich with a layer overlap. Inspection is performed at a 10-kHz scanning speed that takes 16 seconds to scan a 100 × 100 mm^2 area with a scan interval of 0.25 mm. Finally, a comparison is presented between angular-scanning and a linear-scanning-based pulse-echo UPI system. The results show that the proposed system can successfully visualize defects in the inspected specimens.

Keywords: pulse echo laser ultrasound; laser Doppler vibrometer; laser scanning; non-destructive evaluation

1. Introduction

Numerous non-destructive evaluation (NDE) technologies are widely available for structural inspections such as acoustic testing, magnetic field testing, radiography, thermography, and ultrasonic testing. Of all available techniques, ultrasonic testing has the advantages of good resolution, better damage detection, and on-field inspection capabilities (Gholizadeh 2016). Therefore, ultrasonic inspection is used in various structures, such as launch vehicles, aircraft, nuclear systems, and wind turbines, for preventive maintenance (Zhou *et al*. 2016, Saleem 2017, Yim *et al*. 2016). The pulse-echo method is the most popular ultrasonic testing technique, commonly used for thickness measurements and damage localization. In the pulse-echo method, the mechanical vibrations generated by an ultrasonic probe are passed through a structure as sound waves. These waves are reflected back due to disruption and recorded by an ultrasonic sensor. C-scan imaging using the pulse-echo method can also be used for the quantitative visualization of structural delamination or disbonding (ACM handbook 1989). However, conventional immersion and water squirt C-scan technologies perform mainly slow inspections, and cannot be used on complex structures. Due to these practical disadvantages, the C-scan systems cannot be used as an in situ NDE technology.

Laser technologies are extensively used for ultrasound generation because they can conveniently generate high optical energy over a small area (Hutchins 1988). In the early 1990s, a CO2 laser was first used in polymer-matrix composites for ultrasonic wave generation (Chang *et al.* 1993). Other studies have adopted an Nd:YAG laser due to its higher damage threshold and damage-free longitudinal wave generation in composites (Edwards *et al.* 2001, Hong *et al.* 2012). Similarly, researchers have also preferred laser Doppler vibrometers to air-coupled transducers (ACT) for the detection of ultrasonic data because vibrometers do not require the movement of any bulky mechanical parts. Additional advantages of LDV include portability, non-contact measurements, and long-range sensing abilities (Scruby and Drain 1990, Cho *et al.* 2018, Kundu 2003, Truong and Lee 2016, Wdowik *et al.* 2015).

The ultrasonic propagation imager (UPI) exhibits full wavefield techniques by taking the dense grid set of ultrasonic data during a preset duration from an inspected area. Various UPI systems has been developed using different principles of ultrasonic testing. Lee *et al.* (2011), Lee *et al.* (2010), and Chia *et al.* (2009) used guided wave sensing in UPI. A PZT sensor was used as an ultrasonic sensor, while a Q-switched laser along with a galvanometer-type mirror scanner, was used in the laser scanning system to generate lamb waves. Using various damage detection algorithms, the guided-wave UPI was able to inspect in situ,

*Corresponding author, Professor
E-mail: leejrr@kaist.ac.kr
[a] Ph.D. Student
E-mail: habbas33@kaist.ac.kr

ISSN: 1738-1584 (Print), 1738-1991 (Online)

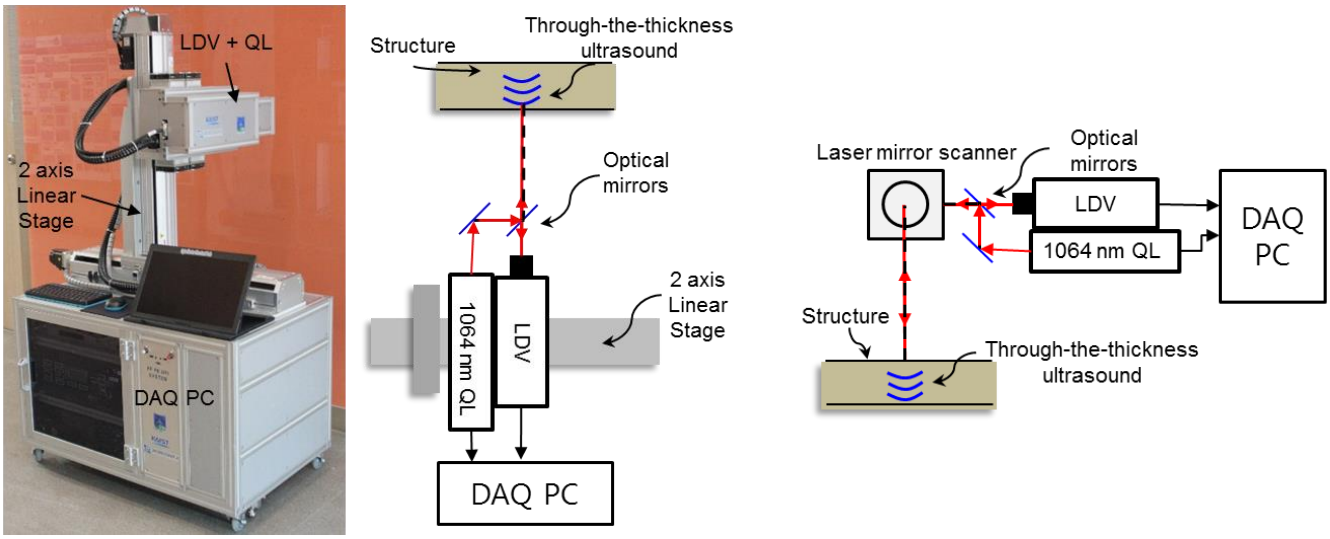

(a) L-PE-UPI (b) A-PE-UPI

Fig. 1 Comparison of bulk wave UPI configurations

long distance, hot targets, and variety of structures. Truong *et al.* (2015) and Truong *et al.* (2016) introduced another upgraded non-contact sensing method using laser Doppler vibrometer in UPI. Furthermore, Hong *et al.* (2016) and Abetew *et al.* (2017) used a pulse-echo method in UPI and produced C-Scan results by non-dispersive, through-the-thickness, longitudinal, ultrasonic wave detection. They used a Q-switched laser and an LDV mounted on a two-axis translation stage to perform raster scans. A Linear-scan Pulse-echo UPI (L-PE-UPI) has the advantage of effectively detecting thickness-related damages and unlike guided-wave UPI, the inspection area of PE-UPI is not limited by wave energy dissipation. Hong *et al.* (2017) made another advancement in UPI technology using the through-transmission mode of ultrasonic testing. In a through-transmission ultrasonic wave propagation imager (TT-UPI), the test specimen was mounted on a translation stage and moved in a raster scan pattern between generation and sensing lasers. Both L-PE-UPI and TT-UPI face several disadvantages due to the translation stage. (1) The maximum scan speed is restricted to 1.8 kHz due to the limitation caused by the motion of the mechanical translation stage. (2) The size of the 2-axis transition stage also makes it impossible to scan surfaces that are challenging to reach. (3) The methods cannot scan vertically inclined surfaces because the translation stage cannot be tilted vertically, and scanning is only possible if the translation stage is parallel to the inspection plane. These issues can be resolved by using a galvanometer-based laser mirror scanner for raster scanning purposes instead of the translation stage because of the fast scan speed, small size, and light weight. Therefore, a PE-UPI system has been developed with a galvanometer laser mirror scanner instead of a translation stage called an angular-scan pulse-echo ultrasonic propagation imager (A-PE-UPI), as shown in Fig. 1.

Previous researchers have used galvanometer-based laser mirror scanners to scan in the pulse-echo ultrasound method. Andrew and Addison (1994) integrated galvanometer mirror scanners into a laser-based ultrasound system. They produced post-processed C-scan images for both flat and contoured composite structures with a very low scan rate of 18 pixels per second at laser pulse repetition rate of 50 Hz. In another study, a laser mirror scanner was used for pulse-echo ultrasonic testing of concrete (Koehler *et al.* 1997). They detected the back wall in the 3D visualization result produced by sensing a Rayleigh wave using a laser Doppler vibrometer. However, the measurement speed was 1.5 s per point, and repetition rates were lower than 50 Hz. Bentouhami *et al.* (2010) and Campagne *et al.* (2013) used an optical scanner in a laser-ultrasonic inspection technology using commercial robots called laser ultrasound for composite inspection (LUCIE). These robots were used to position the scanning head. The generation laser was an atmospheric CO_2 laser with a maximum repetition rate of 400 Hz, and a non-planar ring oscillator was used in combination with fiber laser amplifier for detection. The main advantage of the LUCIE system is the flexibility this system offers due to the robotics; however, its scanning speed is still as low as 4.35 scan points per second. Previous studies and existing technology still do not satisfy the need for a high-speed, real-time and flexible inspection system. Therefore, these issues are addressed in angular-scan pulse-echo ultrasonic propagation imager (A-PE-UPI) technology.

In this paper, an angular-scan pulse-echo ultrasonic propagation imaging system is proposed that employs a 2D galvanometer mirror scanner for high-speed raster scans. Replacing the translation stage with mirror scanner reduces the overall size of the system and increases the flexibility in difficult inspection conditions. With this new configuration, real-time results of through-the-thickness ultrasonic propagation videos at high inspection speeds can be produced. These results can be displayed on-the fly at a very high scanning speed of 10,000 points per second. A Q-switched diode pumped solid state (DPSS) laser is used for

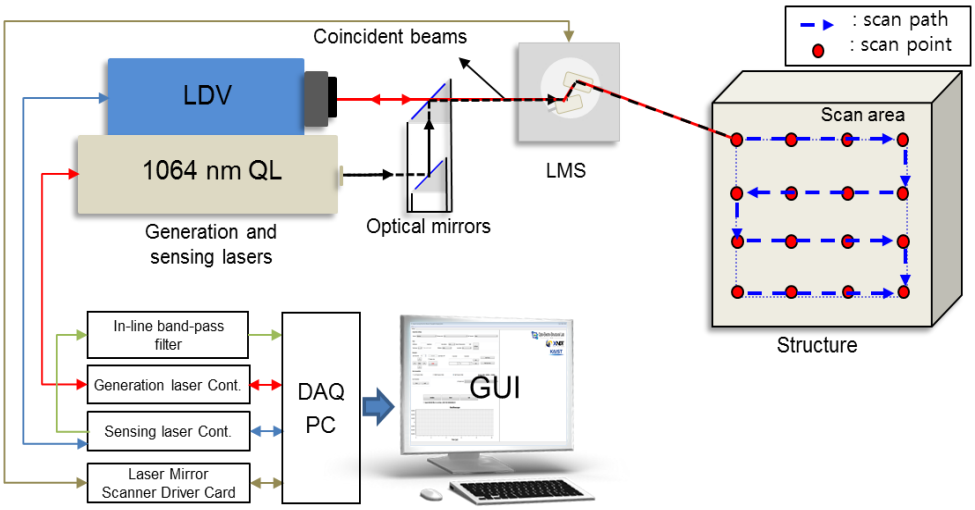

Fig. 2 A-PE-UPI system schematic diagram for raster scanning

generation due to its high damage threshold, and a heterodyne laser interferometer is used for non-contact ultrasonic detection, which can be placed for longer measurement distances. The advantage of this technology is its compactness, flexibility, non-destructive inspection, long-range measurement, non-contact inspection, long-range measurement, non-contact inspection, and fast scanning. The novel technology is tested on an aluminum honeycomb sandwich and carbon fiber reinforced plastic (CFRP) honeycomb sandwich to visualize the structural anomalies due to disbonds and layer overlap.

The remainder of this paper is organized as follows. First, the description of the A-PE-UPI system is presented in Section 2. Next, the experimental and inspection details are discussed in Section 3. Finally, the results obtained using A-PE-UPI are presented and compared with L-PE-UPI in Section 4. The paper ends with conclusions in Section 5.

2. Overview of Angular-scan Pulse-echo Ultrasonic Propagation Imager (A-PE-UPI)

2.1 System description

The A-PE-UPI system consists of a Q-switched laser, a laser Doppler vibrometer, a galvanometer laser mirror scanner, and data acquisition equipment, as shown in Fig. 2. The Q-switched laser (QL) is a 1064-nm diode-pumped solid-state laser with a beam diameter of 0.7 mm; the laser is used for ultrasound generation. The QL has more stable ultrasonic generation performance at higher pulse repetition frequencies (PRF). The maximum PRF of the selected QL that can be operated in the A-PE-UPI system is 10 kHz because, above 10 kHz, the laser pulse energy is too low. The maximum laser pulse energy at 10 kHz is 2.20 mJ. Non-contact ultrasonic sensing is performed using a laser Doppler vibrometer (LDV). In LDV, a helium neon laser serves as a light source, and it generates a linear polarized beam of 633 nm wavelength and 2 mW power. A data acquisition (DAQ) card installed in a PC is used to capture the signal from the LDV. The signal is digitized at a sampling rate of 10 MHz with a signal length of 51.2 μs. Both sensing and generation beams are combined using optics to obtain the pulse-echo through-the-thickness ultrasonic information at each grid-point in the inspection area. This combined beam is passed through a galvanometer-based laser mirror scanner (LMS) to the target structure. The LMS has two mirrors with dialectical high-performance coatings for working wavelengths of 1064 nm and 633 nm. Each mirror is connected to a galvano-motor, and the rotation axes of galvano-motors are orthogonal to each other. These galvano-motors are capable of rotating the mirrors at the maximum angular speed of 70 rad/s within an angular range of ± 20°. During a raster scan, the LMS reflects the combined generation and sensing beam to the target structure.

2.2 Scan procedure

LMS generates a transistor-transistor logic (TTL) signal during scanning, after moving to next scan point. This TTL signal serves as an external trigger to QL. The laser pulse from QL and the data acquisition are synchronized with the TTL signal from the LMS. The scan speed of galvano-motors is sufficient enough to control the pulses emitted by a QL having a pulse repetition rate in the kilohertz regime. Each TTL signal from the LMS is generated during scanning, and the laser beam impinges on the target surface, which generates an ultrasonic wave (Scruby and Drain, 1990). At the same time, LDV measures the velocity of the through-the-thickness longitudinal ultrasonic wave from the same location where it was generated. This measured signal from the LDV is digitized and acquired by the DAQ. Finally, the pulse-echo ultrasonic wave propagation imaging (PE-UWPI) movie is updated. This process continues until scanning is completed, as shown in the flow chart in Fig. 3.

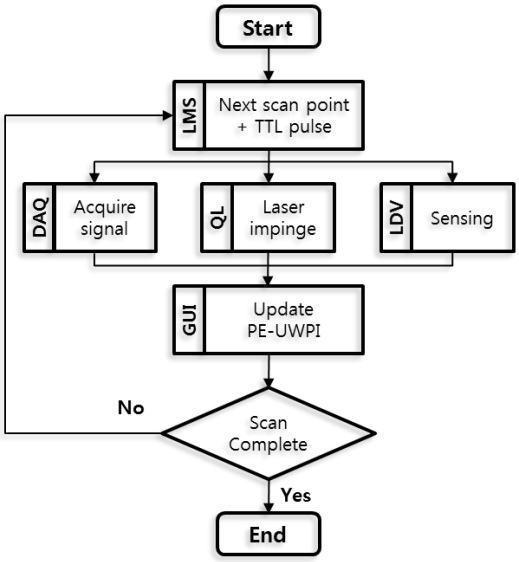

Fig. 3 Flow chart for scanning and data acquisition

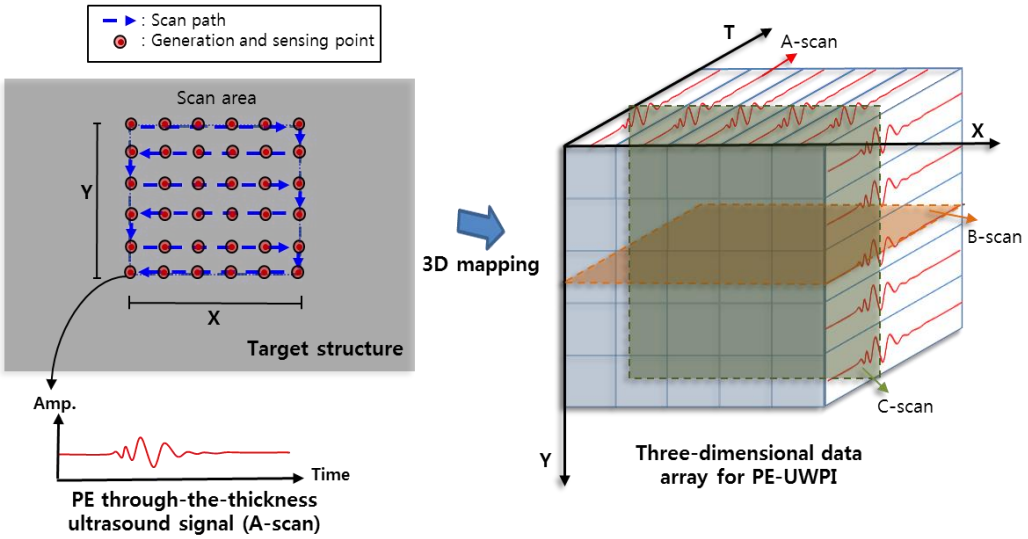

Fig. 4 Pulse-echo ultrasonic wave propagation imaging (PE-UWPI) data mapping

2.3 Pulse-echo ultrasonic wave propagation imaging (PE-UWPI)

The combined generation and sensing beams scan the inspection area in a raster scan pattern. Since the sensing and generation points are theoretically identical, the LDV beam can detect the pulse-echo wave in the longitudinal mode. These pulse-echo waves are collected for each point in the scan grid during raster scanning, and each point is stored in the data acquisition PC. Ultimately, the points are rearranged into a three-dimensional data structure (X×Y×T) to generate a pulse-echo ultrasonic wave propagation video, as shown in Fig. 4. The final mapped data is visualized as intensity maps. Each intensity map is a two-dimensional array of size X×Y, which is equal to the number of points in the scan area. X and V are the number of scan points in the horizontal and vertical directions, while T is the sampling length of the ultrasonic signal. Each scan point of length T in the three-dimensional array represents the A-scan, and each X×T or Y×T two-dimensional map represents B-scan. Similarly, each intensity map of the PE-UWPI video consists of a X×Y two-dimensional array that represents a C-scan image.

If a vector denotes the ultrasonic signal captured at each scan point, the A-scan vector can be represented mathematically.

$$\{S_{x,y}\}_{A-scan} = \begin{pmatrix} S_{x,y}(0) \\ S_{x,y}(1) \\ S_{x,y}(2) \\ \vdots \\ S_{x,y}(N-1) \end{pmatrix} \quad (1)$$

where S_{xy} is the scan point at the x^{th} column and y^{th} row with N number of total samples. The single scan line can also be represented in a matrix, which gives the B-scan matrix shown in Eq. (2).

$$S(y)_{B-scan} = \begin{pmatrix} S_{0,y}(0) & S_{1,y}(0) & \cdots & S_{X-1,y}(0) \\ S_{0,y}(1) & S_{1,y}(1) & \cdots & S_{X-1,y}(1) \\ \vdots & \vdots & \ddots & \vdots \\ S_{0,y}(N-1) & S_{1,y}(N-1) & \cdots & S_{X-1,y}(N-1) \end{pmatrix} \quad (2)$$

$$= \begin{bmatrix} \{S_{0,y}\} & \{S_{1,y}\} & \cdots & \{S_{X-1,y}\} \end{bmatrix} \quad (3)$$

where S(y) is the B-scan matrix at the y^{th} row of the scan area, and y = 0, 1, 2,. .., Y-1. The B-scan gives the image of the cross-section of the test object. Moreover, the C-scan image can also be represented in the matrix form as shown in Eq. (4).

$$S(t)_{C-scan} = \begin{pmatrix} S_{0,0}(t) & S_{1,0}(t) & \cdots & S_{X-1,0}(t) \\ S_{0,1}(t) & S_{1,1}(t) & \cdots & S_{X-1,1}(t) \\ \vdots & \vdots & \ddots & \vdots \\ S_{0,Y-1}(t) & S_{1,Y-1}(t) & \cdots & S_{X-1,Y-1}(t) \end{pmatrix} \quad (4)$$

where S(t) is the C-scan matrix at the t^{th} sample point, and t = 0, 1, 2, . . ., T-1. This C-scan matrix also represents the freeze frame of the pulse-echo ultrasonic wave propagation video. This C-scan is used to visualize the through-the-thickness ultrasonic wave propagation image of the internal structure of the test object. Finally, the complete three-dimensional data structure of the PE-UWPI video can be represented in a 3D matrix as follows.

$$S_{3D} = \begin{pmatrix} \{S_{0,0}\} & \{S_{1,0}\} & \cdots & \{S_{X-1,0}\} \\ \{S_{0,1}\} & \{S_{1,1}\} & \cdots & \{S_{X-1,1}\} \\ \vdots & \vdots & \ddots & \vdots \\ \{S_{0,Y-1}\} & \{S_{1,Y-1}\} & \cdots & \{S_{X-1,Y-1}\} \end{pmatrix} \quad (5)$$

3. Experiment and results

The effectiveness of the angular scan pulse-echo ultrasonic wave propagation imaging (A-PE-UPI) system in non-destructive evaluation application was experimentally verified by applying this technology for the inspection of real structures. Two separate scenarios with different structures were designed for inspection, and the results were compared with the translation-stage-based Linear-scan pulse-echo ultrasonic wave propagation imager (L-PE-UPI). In the first case, an inspection was performed on aluminum honeycomb specimen having disbond and core crush. While in second case, we scanned CFRP honeycomb specimen with layer overlap. Both cases are discussed in detail in this section.

3.1 Aluminum honeycomb structure

Angular scanning was performed using the A-PE-UPI system on the aluminum honeycomb sandwich structure. The aluminum honeycomb consists of 305 × 305 × 0.635 mm^3 aluminum panels and a 9.525 mm thick aluminum core, as shown in Fig. 5. There were disbonds in the specimen due to core damage. Also, the core crush was present inside the honeycomb structure. The rear side of the specimen was inspected first at area A and then at area B. The scan area size was set to 100 × 100 × 0.25 mm^3 for each inspection. This gives total number of 160,000 scan points in one complete scan. The structure was scanned at a 10-kHz pulse repetition rate with 2.2 mJ of pulse energy. The standoff distance between the laser mirror scanner and the specimen was 2.216 m, so the distance between the specimen and the LDV falls in the visibility maxima region. The visibility maxima are the standoff distances of the LDV at which the signal level is maximum, and the maxima recurs every 204 mm. The LDV sensitivity was set to 5 mm/s/V, and its internal filter range was set at the frequency of 1.5 MHz. The LDV signal was filtered at the bandpass range of 50 - 200 kHz prior to acquisition. The experimental setup for the honeycomb sandwich aluminum structure is shown in Fig. 6.

The pulse-echo UWPI videos were generated for both scan areas A and B to visualize the specimen damage. These videos show the internal structure of the aluminum honeycomb in time as soon as the ultrasonic wave in the longitudinal mode passes through-the-thickness. The C-scan images were also captured from the UWPI movie at 16.5 μs and were compared to the results obtained from L-PE-UPI, as shown in Fig. 7. The L-PE-UPI results were generated at a 1.8 kHz scan speed that was achieved by setting the two-axis translation stage at 450 mm/s.

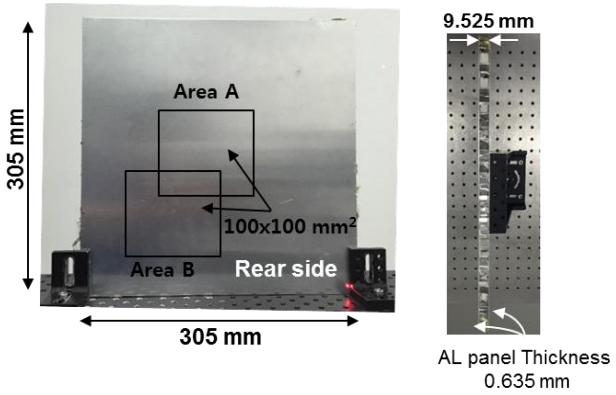

(a) Rear view (b) Side view

Fig. 5 Aluminum honeycomb sandwich structure

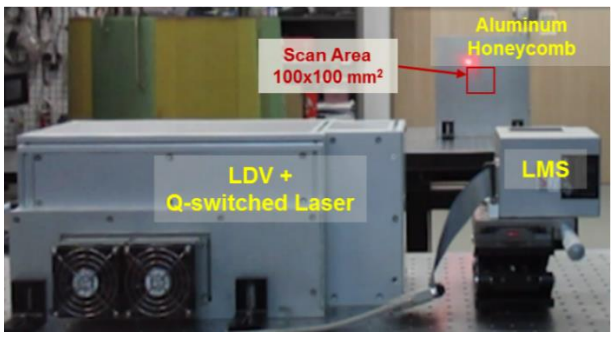

Fig. 6 Experimental configuration for aluminum honeycomb sandwich inspection

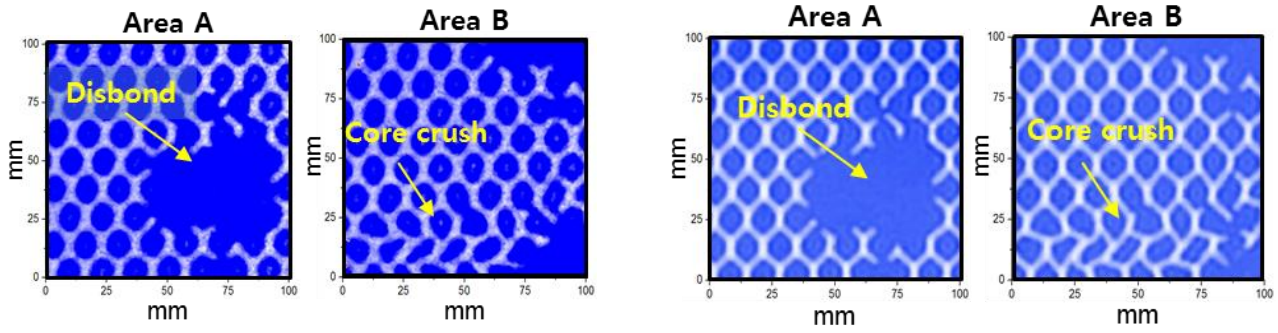

(a) A-PE-UPI results (b) L-PE-UPI results

Fig. 7 Comparison of aluminum honeycomb structure inspection results

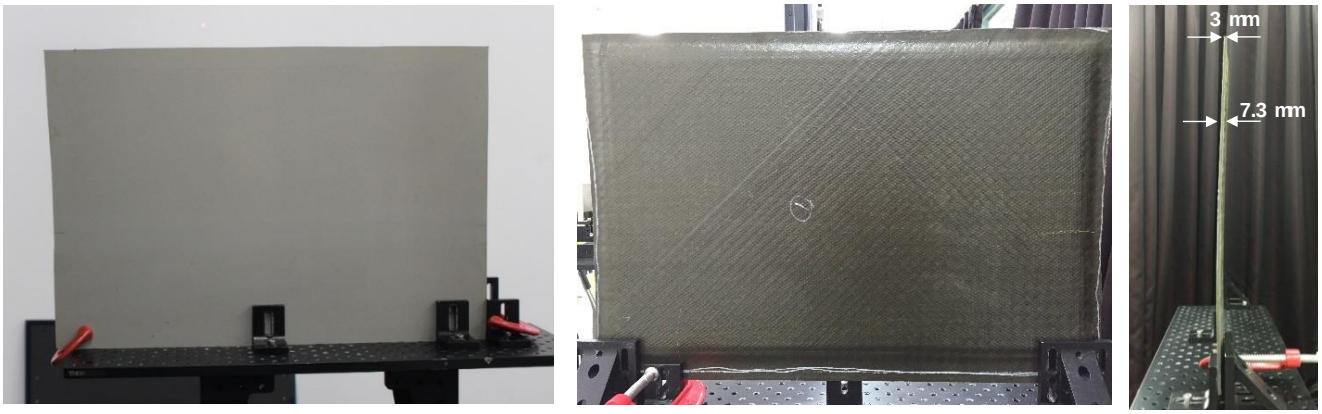

(a) Front view (a) Back view (a) Side view

Fig. 8 CFRP honeycomb structure

The laser pulse energy used in L-PE-UPI inspection was set to 5.6 mJ. The comparison results show good correlation between the two techniques. The results from both scan areas clearly exhibit the disbond and core crush, and they also agree with the translation-stage-based PE-UWPI result.

3.2 CFRP honeycomb structure

In another case, a CFRP honeycomb structure, used in a UAV skin panel, was inspected using the A-PE-UPI system. It had 0.4363 mm thick CFRP panels with Nomex honeycomb having a core thickness of 6.35 mm, as shown in Fig. 8. The structure has a layer overlap on the top left corner of the front side. An area of 100 × 100 × 0.25 mm^3 was scanned at a 10-kHz pulse repetition rate from a 1.8 m LMS standoff distance. The generation laser pulse energy was set at 2.2 mJ, and the LDV sensing range was set to 5 mm/s/V. The bandpass filter range of 50 - 200 kHz was also applied to the LDV signal. The inspection setup for the CFRP honeycomb structure is shown in Fig. 9.

The laser C-scan result was obtained from the PE-UWPI video generated imediately after inspection. The freeze-frame of the PE-UWPI video was captured at 10.23 µs. The anomaly due to layer overlap in the CFRP panel can be easily visualized from the result generated by angular scanning, as shown in Fig. 10(a). The comparison was also made between A-PE-UPI and L-PE-UPI for CFRP honeycomb structure, as shown in Fig. 10. For comparison, the C-scan produced using L-PE-UPI was generated with 5.6 mJ laser pulse energy at a 1.8 kHz pulse repetition rate. The layer overlap location was identical in both systems. Therefore, the result from L-PE-UPI justifies the damage detection capability of A-PE-UPI.

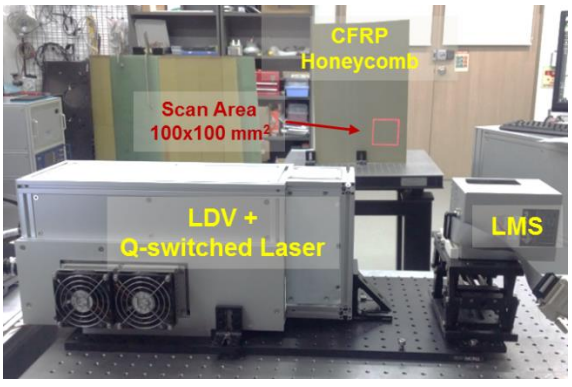

Fig. 9 Experimental configuration for aluminum honeycomb sandwich inspection

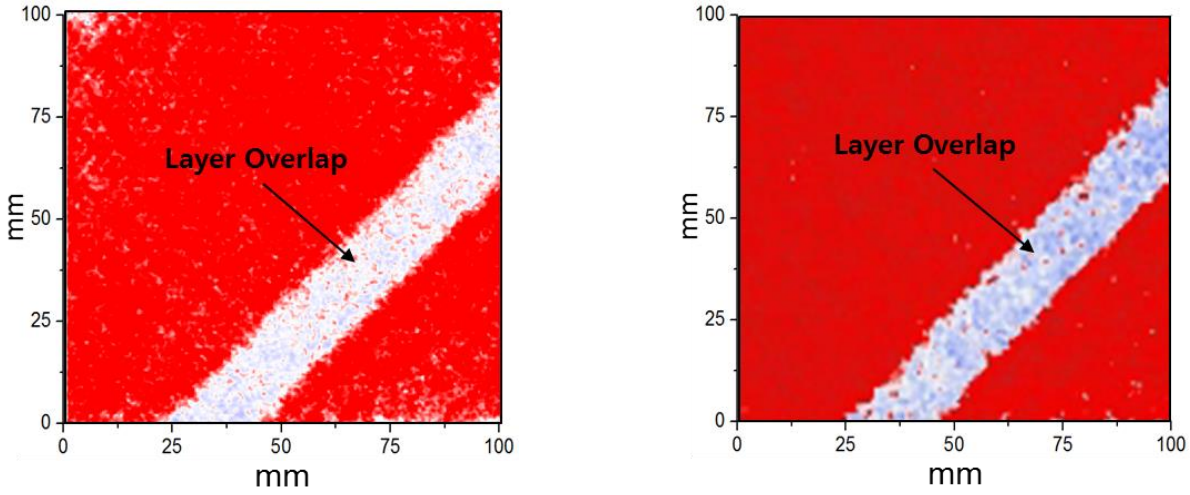

(a) A-PE-UPI results (b) L-PE-UPI results

Fig. 10 Comparison of aluminum honeycomb structure inspection results

The linear translation stage, which was used in the L-PE-UPI system, required 7 minutes and 14 seconds to scan 400 × 400 points to generate a PE-UWPI movie at 1.8 kHz.

The maximum scan speed was limited to 1.8 kHz in the 2-axis translation stage. In addition, mechanical scanning also added extra time due to the acceleration and deceleration of the stage while moving to the next row. The acceleration and deceleration of the mechanical stage and stepping into a new row added up to 0.95 seconds to the scanning time per row. This finding indicates that, for a scan area of 100 × 100 × 0.25 mm^3, an extra 6 minutes and 17 seconds will be taken due to mechanical scanning. In contrast, galvanometer technology features very high torque with small electrical inductance to provide higher scanning speed and the fastest step response times (Aylward 1999). Therefore, this speed limitation caused by a bulky two-dimensional translation stage and the mechanical motion was not observed when optical scanning was performed. In the case of high-speed angular scanning using A-PE-UPI, the same number of points were scanned and acquired 27 times faster. It took only 16 seconds to inspect a scan area with 16,000 points at a 10-kHz scan speed.

4. Conclusions

In this paper, the angular scan pulse-echo laser ultrasonic propagation imager (A-PE-UPI) was proposed for the accelerated non-destructive inspection of aerospace structures. The system detects the through-the-thickness longitudinal ultrasonic bulk waves generated by a 1064-nm DPSS laser using a non-contact based LDV. Experiments were conducted with two different structures as follows: (1) aluminum honeycomb sandwich and (2) CFRP honeycomb. The results generated with angular scanning in A-PE-UPI showed good correlation with the previous mechanical scanning method with the two-axis translation stage used in L-PE-UPI.

The integration of the galvano-motorized mirror scanner allowed the combined generation and sensing beam to rapidly scan the surface. This new scanning technique enabled the system to scan up to 10,000 points per second. Experiments showed that for an inspection of a 100 × 100 × 0.25 mm^3 area, A-PE-UPI took only 16 seconds to complete the inspection. The same scan area took 7 minutes and 14 seconds when scanned with L-PE-UPI. This advancement in scanning speed can save up to 96.3 % of inspection time.

A-PE-UPI offers several advantages over other pulse-echo based systems including the following: (1) it provides rapid inspection capability, (2) it is fully non-contact and non-destructive, (3) its portable UPI head size allows for inspection in challenging environments, (4) its angular scanning combines beams to inspect through a narrow area of sight to the target, and (5) its low-weight allows the UPI head to be mounted on various stages to improve accessibility to targets and optimize 3D shaped targets.

Acknowledgments

This paper was supported by the Technology Innovation Program (10074278) funded by the Ministry of Trade, Industry & Energy (MI, Korea) and the National Research Foundation of Korea Grant (NRF-2017R1A5A1015311) funded by the Ministry of Science and ICT.

References

Abetew, A.D., Hong, S.C., Lee, J.R., Baek, S. and Ihn, J.B. (2017), "Remote defect visualization of standard composite coupons using a mobile pulse-echo ultrasonic propagation imager", *Adv. Compos. Mater.*, **26**(1), 15-27.

ASM Handbook (1989), Volume 17: Nondestructive Evaluation and Quality Control, ASM International.

Aylward, R.P. (1999), "Advances and technologies of

galvanometer-based optical scanners", In Proc. SPIE, 3787, 158-164.
Bentouhami, F., Campagne, B., Cuevas, E., Drake, T., Dubois, M., Fraslin, T., Piñeiro, P., Serrano, J. and Voillaume, H. (2010), "LUCIE-A flexible and powerful Laser Ultrasonic system for inspection of large CFRP components", *Proceedings of the 2nd International Symposium on Laser Ultrasonics*, Talence, France.
Campagne, B., Voillaume, H., Gouzerh, L. and Bentouhami, F. (2013), "Laser ultrasonic developments for NDT of aeronautic composite parts", *Proceedings of the 13th International Symposium on Nondestructive Characterization of Materials (NDCM-XIII)*, Le Mans, France.
Chang, F.P., Drake, T.E., Osterkamp, M.A., Monchalin, J.P., Heon, R., Bouchard, P., Padioleau, C., Froom, D.A., Frazier, W. and Barton, J. (1993), "Laser ultrasonic inspection of honeycomb aircraft structures", *Review of Progress in Quantitative NDE*, **12**, Plenum Press, New York, 611-616.
Chia, C.C., Lee, J.R. and Shin, H.J. (2009), "Hot target inspection using a welded fibre acoustic wave piezoelectric sensor and a laser-ultrasonic mirror scanner", *Measur. Sci. Technol.*, **20**(12), 127003.
Cho, S., Lee, J. and Sim, S.H. (2018), "Comparative study on displacement measurement sensors for high-speed railroad bridge", *Smart Struct. Syst.*, **21**(5), 637-652.
Edwards, C., Stratoudaki, T., Dixon, S. and Palmer, S. (2001), "Laser generated ultrasound: efficiency and damage thresholds in carbon fibre reinforced composites", *IEE Proceedings-Science, Measurement and Technology*, **148**(4), 139-142.
Gholizadeh, S. (2016), "A review of non-destructive testing methods of composite materials", *Procedia Struct. Integrity*, **1**, 50-57.
Hong, S.C., Abetew, A.D., Lee, J.R. and Ihn, J.B. (2016), "Three dimensional evaluation of aluminum plates with wall-thinning by full-field pulse-echo laser ultrasound", *Optics and Lasers in Engineering*.
Hong, S.C., Lee, J.R. and Jung-il, k. (2017), "In process quality control of F-16 brake disk using in-process through-transmission ultrasonic propagation imaging system", In *Korean Society of Nondestructive Testing (KSNT)*, Daegu, South Korea, May.
Hong, S.C., Lee, J.R., Chong, S.Y. and Park, C.Y. (2012), "Effect of Laser Pulse Fatigue on the Mechanical Characteristics of a CFRP Plate", *Appl. Mech. Mater.*, **225**, 121-126.
Hutchins, D.A. (1988), Ultrasonic generation by pulsed lasers, *Phys. Acoust.*, **18**, 21-123.
Koehler, B., Hentges, G. and Mueller, W. (1997), "A novel technique for advanced ultrasonic testing of concrete by using signal conditioning methods and a scanning laser vibrometer", *Proceedings of the 4th International Conference on Non-destructive Testing in Civil Engineering*, Liverpool, Uk.
Kundu, T. (2003), Ultrasonic Nondestructive Evaluation: Engineering and Biological Material Characterization, CRC press, New York, NY, USA.
Lee, J.R., Jeong, H., Ciang, C.C., Yoon, D.J. and Lee, S.S. (2010), "Application of ultrasonic wave propagation imaging method to automatic damage visualization of nuclear power plant pipeline", *Nuclear Engineering and Design*, **240**(10), 3513-3520.
Lee, J.R., Shin, H.J., Chia, C.C., Dhital, D., Yoon, D.J. and Huh, Y.H. (2011), "Long distance laser ultrasonic propagation imaging system for damage visualization", *Opt. Laser. Eng.*, **49**(12), 1361-1371.
McKie, A.D. and Addison, R.C. (1994), "Practical considerations for the rapid inspection of composite materials using laser-based ultrasound", *Ultrasonics*, **32**(5), 333-345.
Saleem, M. (2017), "Study to detect bond degradation in reinforced concrete beams using ultrasonic pulse velocity test method", *Struct. Eng. Mech.*, **64**(4), 427-436.
Scruby, C.B. and Drain, L.E. (1990), Laser Ultrasonics Techniques and Applications, CRC Press, New York, NY, USA.
Truong, C.T., Kang, D.H., Lee, J.R. and Farrar, C.R. (2015), "Comparative study of laser Doppler vibrometer and capacitive air-coupled transducer for ultrasonic propagation imager and the new development of an efficient ultrasonic wavenumber imaging algorithm", *Strain*, **51**(4), 332-342.
Truong, T.C. and Lee, J.R. (2016), "SNR enhancement for composite application using multiple Doppler vibrometers based laser ultrasonic propagation imager", *Opt. Laser. Eng.*, **84**, 82-88.
Wdowik, R., Nazarko, P. and Porzycki, J. (2015), "Application of eddy current sensor System and LDV device for ultrasonic vibrations measurements", *In Mechatronics-Ideas for Industrial Application*, Springer, Cham, 407-415.
Yim, H.J., Park, S.J., Kim, J.H. and Kwak, H.G. (2016), "Evaluation of freezing and thawing damage of concrete using a nonlinear ultrasonic method", *Smart Struct. Syst.*, **17**(1), 45-58.
Zhou, W., Li, H. and Yuan, F.G. (2016), "An anisotropic ultrasonic transducer for Lamb wave applications", *Smart Struct. Syst.*, **17**(6), 1055-1065.